



**QUEEN'S
UNIVERSITY
BELFAST**

Comparative assessment of visible light and UV active photocatalysts by hydroxyl radical quantification

Nagarajan, S., Skillen, N. C., Fina, F., Zhang, G., Randhorn, C., Lawton, L. A., Irvine, J. T. S., & Robertson, P. K. J. (2017). Comparative assessment of visible light and UV active photocatalysts by hydroxyl radical quantification. *Journal of Photochemistry and Photobiology A: Chemistry*, 334, 13-19.
<https://doi.org/10.1016/j.jphotochem.2016.10.034>

Published in:

Journal of Photochemistry and Photobiology A: Chemistry

Document Version:

Peer reviewed version

Queen's University Belfast - Research Portal:

[Link to publication record in Queen's University Belfast Research Portal](#)

Publisher rights

© 2016 Elsevier Ltd. This manuscript version is made available under the CC-BY-NC-ND 4.0 license <http://creativecommons.org/licenses/by-nc-nd/4.0/> which permits distribution and reproduction for non-commercial purposes, provided the author and source are cited.

General rights

Copyright for the publications made accessible via the Queen's University Belfast Research Portal is retained by the author(s) and / or other copyright owners and it is a condition of accessing these publications that users recognise and abide by the legal requirements associated with these rights.

Take down policy

The Research Portal is Queen's institutional repository that provides access to Queen's research output. Every effort has been made to ensure that content in the Research Portal does not infringe any person's rights, or applicable UK laws. If you discover content in the Research Portal that you believe breaches copyright or violates any law, please contact openaccess@qub.ac.uk.

Open Access

This research has been made openly available by Queen's academics and its Open Research team. We would love to hear how access to this research benefits you. – Share your feedback with us: <http://go.qub.ac.uk/oa-feedback>

1 **Comparative assessment of visible light and UV active photocatalysts by hydroxyl**
2 **radical quantification**

3 Sanjay Nagarajan^{1*}, Nathan C. Skillen¹, Federica Fina², Guan Zhang², Chamnan
4 Randorn², Linda A. Lawton³, John T.S. Irvine² and Peter K.J. Robertson^{1*}

5 ¹ Centre for the Theory and Application of Catalysis (CenTACat), School of Chemistry
6 and Chemical Engineering, Queen's University Belfast, David Keir Building, Stranmillis
7 Road, Belfast, BT9 5AG, United Kingdom;

8 ² JTSI Group, University of St. Andrews, School of Chemistry, Purdie Building, North
9 Haugh, St Andrews, KY16 9ST, United Kingdom;

10 ³ School of Pharmacy and Life sciences, Sir Ian Wood Building
11 Robert Gordon University, Garthdee Road, Aberdeen, AB10 7GJ, United Kingdom

12 *Corresponding authors, *p.robertson@qub.ac.uk*; *snagarajan01@qub.ac.uk*, Tel: +44
13 (0) 28 9097 4627

14

15 **ABSTRACT**

16 A simple method for determining hydroxyl radical yields on semiconductor
17 photocatalysts is highly desirable, especially when comparing different photocatalyst
18 materials. This paper reports the screening of a selection of visible light active
19 photocatalysts such as Pt-C₃N₄, 5% LaCr doped SrTiO₃, Sr_{0.95}Cr_{0.05}TiO₃ and Yellow
20 TiO₂ and compares them against WO₃ and ultra violet (UV) light activated TiO₂ P25
21 (standard commercial catalysts) based on their oxidative strengths (OH radical
22 producing capability) using a well-studied chemical probe – coumarin. 7-
23 hydroxycoumarin, the only fluorescent hydroxylation product of this reaction can then
24 be measured to indirectly quantify the OH radicals produced. P25 under UV light
25 produced the highest concentration of OH radicals (16.9 μM), followed by WO₃ (0.56
26 μM) and Pt-C₃N₄ (0.25 μM). The maximum OH radical production rate for P25, WO₃

27 and Pt-C₃N₄ were also determined and found to be 35.6 μM/hr, 0.28 μM/hr and 0.88
28 μM/hr respectively. The other visible light activated photocatalysts did not produce any
29 OH radicals primarily as a result of their electronic structure. Furthermore, it was
30 concluded that, if any visible light absorbing photocatalysts are to be fabricated in
31 future for the purpose of photocatalytic oxidation, their OH radical producing rates (and
32 quantities) should be determined and compared to P25.

33 **Keywords:** Photocatalyst, visible light photocatalysts, OH radical, coumarin, P25.

34

35

36

37

38

39

40

41

42

43

44

45

46

47

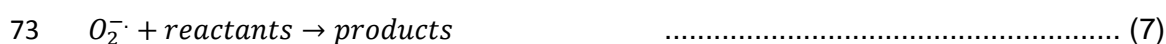
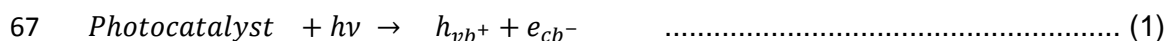
48

49

50 1. INTRODUCTION

51 Photocatalysis has gained significant interest since the early publication by
52 Fujishima and Honda in 1972, demonstrating the potential of splitting water over TiO₂
53 [1]. Since this publication, photocatalysis has been applied to a broad range of fields
54 including waste water treatment, microbe destruction, toxin removal, energy production
55 and air treatment. [2-8]. The mechanism of photocatalysis has been well documented
56 and can be generally represented by the equations shown in reactions 1-9 [9,10]. The
57 formation of surface radical species such as superoxide (O₂^{-·}) and hydroxyl radicals
58 (OH[·]) play a key role in a number of photocatalytic pathways and as such their
59 identification and quantification is a key consideration. As shown in reaction 2, OH
60 radicals are primarily generated from the reaction between valence band holes (h_{vb+})
61 and hydroxyl ions on the catalyst surface. An indirect pathway, via O₂^{-·}, also results in
62 OH radical formation, as shown in reactions 3-6. The efficiency of OH radicals in
63 photocatalytic reactions is predominantly based on their strong oxidising potential of
64 2.8 V (vs NHE) [11]. The non-selective nature of these reactive oxygen species also
65 aids rapid degradation of various pollutants and organic contaminants [3,7,11-16].

66





76 where, h_{vb}^+ represents VB holes and e_{cb}^- means CB electrons.

77

78 Newly developed photocatalytic technologies and materials have often utilised
79 model compounds and screening methods to assess their performance [17-20].
80 Common evaluation methods reported in the literature include the decomposition of
81 dyes such as methylene blue (ISO test 10678:2010), or degradation of organic
82 pollutants such as 4-chlorophenol or toluene [17-20]. These procedures are often
83 coupled with the corresponding calculated photonic efficiencies and quantum yields to
84 evaluate overall efficiency. While these methods can be effective in identifying the
85 specific photocatalytic performance of a material in relation to a fingerprint compound,
86 they provide little information regarding the production of OH radicals involved within
87 the mechanism. Therefore, the requirement for a simple and robust method of radical
88 quantification for screening the oxidative potential of catalysts has significantly
89 increased. The challenge in OH radical quantification lies in both the non-selective
90 nature and short lifetime (~ 1 nanosecond) of the radical, which restricts the possibility
91 of direct quantification [21]. Consequently, a range of methods have been developed
92 such as emission spectroscopy, laser induced fluorescence, electron spin resonance,
93 spin trap and chemical probes or quencher based methods to quantify OH radicals [21-
94 37].

95

96 The use of a chemical probe to capture OH radicals presents a potentially efficient
97 way to measure the radical due to the low cost, rapid analysis time and reproducibility
98 of the method. Monitoring a probe compound through spectroscopy allows the
99 concentration of OH radicals to be calculated based on stoichiometric ratios of products
100 formed. A recently reported *in vivo* technique utilised a nanoprobe comprising of a
101 nanoparticle and azo dye in order to quantify OH radicals in the femtomolar range [37].

102 Here the nanoparticle was used as an energy donor and the modified orange was used
103 as an OH radical capturing ligand molecule (and the energy acceptor).

104

105 Dimethyl sulfoxide (DMSO) based methods for OH radical capture have also been
106 utilised in the past to quantify these species via the formation of formaldehyde
107 [28,29,31]. The formation of CH₄ in a closed system coupled with O₂ bubbling however
108 reduces the suitability of utilising DMSO as a probe molecule.

109

110 In the past, OH radical quantification has been carried out for various commercially
111 available photocatalysts, photo-Fenton's reaction and other modified TiO₂ based visible
112 light photocatalysts with either coumarin or terephthalic acid as probe molecules
113 [21,23,31-36,38,39]. Both compounds are capable of acting as OH radical traps by
114 forming fluorescent products as result of reacting with the radical species. Terephthalic
115 acid has been investigated in a study by Ishibashi *et al.* which achieved an OH radical
116 concentration of 7×10^{-5} M based on the measurement of 2-hydroxyterephthalic acid
117 [35]. In addition to the use of terephthalic acid as a probe molecule, coumarin has been
118 used in a number of studies to determine the concentration of OH radicals produced
119 from TiO₂ at relatively high loadings of 1 to 5 g/L [21,23,40]. For instance, Czili *et al.*
120 used 100 μ M coumarin as the probe molecule to capture OH radicals under a 40 W UV
121 lamp. They determined a maximum OH radical production rate of 23.39 μ M/g/hr
122 (calculated from their reported 7-hydroxycoumarin rates) with 1 g/L TiO₂ P25
123 photocatalyst.

124

125 This paper utilises coumarin as a hydroxyl radical trap and reports the screening of
126 a selection of visible light responsive photocatalysts under low power illumination
127 based on their OH radical producing capability. In contrast to previous reports, which
128 concentrated on quantifying the OH radicals produced from TiO₂, other commercially

129 available and a few synthesised photocatalysts [21,23,31,40], this work focusses on
130 assessing the oxidative strength of visible light photocatalysts Pt-C₃N₄, 5% LaCr
131 doped SrTiO₃, Sr_{0.95}Cr_{0.05}TiO₃ (referred to as Cr-SrTiO₃ from here on) and yellow TiO₂
132 and compares them against commercial TiO₂ P25 and WO₃ for evaluation. In addition,
133 a low catalyst loading was used to highlight efficient OH radical formation can be
134 achieved without requiring large quantities of powdered catalyst.

135

136 **2. EXPERIMENTAL PROCEDURE**

137 **2.1 Materials**

138 Coumarin and 7-hydroxycoumarin were purchased from Tokyo Chemical Industry
139 UK Ltd, while TiO₂ P25 was purchased from Degussa (now Evonik industries) and WO₃
140 nano powders were purchased from Sigma Aldrich. All commercial chemicals were
141 used as received. The catalysts Pt-C₃N₄ [41], 5% LaCr doped SrTiO₃, Cr-SrTiO₃ and
142 yellow TiO₂ [42] were synthesised at the school of chemistry, University of St. Andrews,
143 using methods cited in the literature [41-43].

144

145 **2.2 Characterisation of Photocatalysts**

146 WO₃, LaCr-SrTiO₃ and Cr-SrTiO₃ were characterised by X-Ray diffraction (XRD)
147 and UV-Visible absorption. XRD analysis of powders was examined on a SToe
148 STADI/P powder diffractometer. Incident radiation was generated using a Cu k_α source
149 (λ=1.54056 Å). Diffuse reflectance spectra were collected on a JASCO-V550 UV-
150 visible spectrophotometer. The characterisation of Pt-C₃N₄ and yellow TiO₂ has been
151 reported elsewhere in literature [41,42].

152

153 **2.3 Photocatalytic experiments**

154 All photocatalytic experiments were performed in closed screw cap bottles. The
155 reaction solution was composed of 100 ml of 100 μM coumarin along with 10 mg of

156 photocatalyst (0.1 g/L). A magnetic stirrer bar was placed inside the bottle and the
157 bottle was then placed on a magnetic stirrer at a distance of 11 cm from a 36 W
158 compact fluorescent non-integrated visible lamp (Philips, colour code 830) or a 36 W
159 UV lamp (Philips, Cleo lamps). The spectral outputs of the lamps were measured by a
160 StellaNet spectrometer and the spectra are shown in the supplementary material
161 (Figure S1). Prior to illumination, the reaction solution was stirred in the dark to allow a
162 state of equilibrium to be reached. The length of time required in the dark was
163 calculated from the control experiments conducted in the absence of light. During
164 irradiation, samples (3 mL) were taken at dedicated time intervals for a maximum of
165 120 mins. Samples were filtered through a 0.22 μm Millex syringe filter prior to
166 analysis. Coumarin absorbance was monitored using a Cary 300 Scan, UV-Visible
167 Spectrophotometer at 277 nm, with a scan rate of 400 nm/min. 7-hydroxycoumarin
168 fluorescence was measured in a PerkinElmer LS 50B luminescence
169 spectrophotometer, using an excitation wavelength of 332 nm and emission
170 wavelength at 456 nm [21]. The excitation and emission slit width was 4 mm and the
171 scan rate was 200 nm/min. A sample UV/Visible and fluorimeter spectra, with peaks at
172 277 nm and 456 nm respectively, are shown in the supplementary material Figure S2
173 and Figure S3. All experiments were performed in triplicate.

174

175 **2.4 OH radical quantification**

176 OH radicals were quantified based on a modified method described by Zhang *et al.*
177 [38] and according to equation 1. The concentration of OH radicals was calculated by
178 assuming that 6.1 % of total OH radicals were captured as 7-hydroxycoumarin. The
179 stoichiometric ratio of one mole of OH radical consumed for the production of one mole
180 of 7-hydroxycoumarin was used [23]. The total number of OH radicals produced over
181 time during this photocatalytic process was calculated using the following equation.

182

183 $X = \left\{ \frac{A}{6.1\%} - B \right\}$ Equation 1

184

185 Where, X is the total OH radical concentration (μM) produced during photocatalysis, A
186 is the mean 7-hydroxycoumarin concentration (μM) and B is the amount of OH radicals
187 (μM) produced during the light control experiments. The concentration of coumarin and
188 7-hydroxycoumarin was calculated using a standard curve of known concentrations as
189 shown in the supplementary material (Figure S4, Figure S5 and Figure S6).

190

191 **3. RESULTS AND DISCUSSION**

192 **3.1 Characterisation of Photocatalysts**

193 XRD patterns of WO_3 , Cr-SrTiO_3 and LaCr-SrTiO_3 samples were determined as
194 shown (Figure 1). The commercial WO_3 nanoparticles exhibited a typical crystallized
195 monoclinic phase structure, and the Cr-doped and La,Cr-co-doped SrTiO_3 samples
196 possessed homogeneous crystallized cubic perovskite structures, with no impurity
197 phase found for either of the doped samples and these results were consistent with
198 literature [44,45]. In the co-doped samples, since La and Cr substitute the Sr and Ti,
199 respectively, and the radius of La is similar with that of Sr while the radius of Cr was
200 similar to that of Ti, the peak positions of the Cr-SrTiO_3 and LaCr-SrTiO_3 samples are
201 not shifted compared to those of pure SrTiO_3 .

202

203 **Figure 1.**

204

205 In the UV-visible absorption spectra of WO_3 , Cr-SrTiO_3 and LaCr-SrTiO_3 (Figure
206 2), WO_3 exhibited visible light absorption up to 470 nm, which corresponds to the band-
207 gap energy of ca. 2.64 eV. SrTiO_3 , however, has no absorption in the visible light
208 region (bandgap of 3.75 eV) and metal-doping has been shown to be a feasible
209 method for extending the light absorption of SrTiO_3 into the visible region [46]. Doping

210 of Cr into the A-site of SrTiO₃ induces an absorption band in the visible region centred
211 at around 450 nm (Figure 2). The visible light absorption is ascribed to the electron
212 excitation from the Cr doping levels formed above the valence band of SrTiO₃ to the
213 conduction band of SrTiO₃ [43]. It was reported that La, Cr- co-doped SrTiO₃ showed
214 enhanced photocatalytic performance compared to the single Cr-doped SrTiO₃ due to
215 the inhibition of the formation of Cr⁶⁺ species in the B site [43]. Therefore, a co-doped
216 sample, LaCr-SrTiO₃ was prepared by the same method. The visible light absorption of
217 LaCr-SrTiO₃ was significantly enhanced compared to the Cr-SrTiO₃, with two strong
218 absorption peaks centred at around 450 nm and 650 nm in the visible light region. In
219 the case of co-doping, more intermittent doping levels are formed within the band-gap
220 of SrTiO₃ compared to the single Cr doped SrTiO₃, which results in the visible light
221 absorption.

222

223 **Figure 2.**

224

225 **3.2 Photocatalytic OH radical production**

226 **3.2.1 UV light photocatalysis on P25**

227 P25 has been one of the most extensively investigated and most active
228 commercially available photocatalysts under UV irradiation and therefore was used as
229 a benchmark for comparison in this study. Although, recent studies have reported that
230 nano-spherical InCrO₄-loaded TiO₂ and TiO₂ nanospheres deposited on graphene
231 performed better than P25 for OH radical production and dye degradation upon UV
232 irradiation [47,48], to date P25 is still regarded as the benchmark. The photocatalytic
233 hydroxylation of coumarin over P25 under UV light and subsequent formation of 7-
234 hydroxycoumarin is shown in Figure 3. The production of 7-hydroxycoumarin under
235 these conditions equates to a peak OH radical concentration of 16.9 μM after 45 mins.
236

237 **Figure 3.**

238 As shown in the figure, near complete degradation (97 %) of coumarin was
239 achieved after 120 mins irradiation. This level of degradation was likely to result from
240 the increased adsorption of coumarin onto the catalyst, which facilitated the reaction
241 with surface bound OH radicals. The role of surface bound radicals and those that are
242 present in bulk has been highlighted in a previous publication by Li *et al.* [49], who
243 investigated acid orange oxidation over TiO₂ P25 and AgBr. This group investigated
244 the quenching of OH radicals at the catalyst surface and in bulk in order to demonstrate
245 that surface bound species were the predominant radicals in the oxidation pathway.
246 This observation confirmed that increased adsorption of the substrate on the catalyst
247 surface can significantly increase the degradation efficiency.

248

249 Figure 3 also shows the profile of 7-hydroxycoumarin production and
250 decomposition which indirectly indicates the quantity of OH radicals generated. 7-
251 hydroxycoumarin concentration peaked at 45 minutes, with a maximum concentration
252 of 1.045 μM, which was equivalent to 16.9 μM OH radicals (as calculated from
253 equation 1). It was observed that an average production rate of 1.8 μM/hr was
254 achieved during the first 45 mins, followed by an average degradation rate of 0.46
255 μM/hr during the latter stages of irradiation. The decrease in concentration of 7-
256 hydroxycoumarin could also be attributed to the presence of superoxide radicals as
257 reported by Czili and Horvath [23].

258

259 Several reports have suggested the kinetics for 7-hydroxycoumarin generation
260 from coumarin with P25 under UV irradiation are zero order [21,23,38,50-52], however,
261 a number of these investigations also used a high concentration of both catalyst and
262 coumarin. Furthermore, it has been suggested that at higher concentrations of
263 coumarin (>100 μM), more UV light is absorbed by this probe and not the catalyst,

264 which results in a low 7-hydroxycoumarin and OH radical production rate [23]. In the
265 present study, K_{app} which is the rate constant for the formation of 7-hydroxycoumarin
266 was calculated to be 0.0234 $\mu\text{M}/\text{min}$ whereas K_{dis} , the rate constant for the
267 disappearance of 7-hydroxycoumarin was calculated to be 0.0135 $\mu\text{M}/\text{min}$. In this study
268 we have established that both, production and degradation of 7-hydroxycoumarin
269 followed zero order kinetics, which is agreement with previous studies.

270

271 **3.2.2 Visible light photocatalysis**

272 A number of visible light catalysts were also selected for comparison against P25
273 TiO_2 . While the synthesised catalysts all possessed energy band gaps that supported
274 visible light activation, only WO_3 and $\text{Pt-C}_3\text{N}_4$ had energy band potentials (valence
275 band at 3.2 V and 1.4 V respectively and conduction band at 0.2 V and -1.3 V
276 respectively) that would facilitate OH radical formation either directly or indirectly as
277 mentioned in reactions 2–6. Catalysts LaCr-SrTiO_3 , Cr-SrTiO_3 and yellow TiO_2 (valence
278 bands at 2.7 V, 2.7 V and 2.6 V respectively and conduction bands at -0.1 V for all the
279 three photocatalysts) were selected to monitor if 7-hydroxycoumarin was formed even
280 when the electronic structure of the catalyst was not suited to the redox potential of the
281 reaction.

282

283 The photocatalytic hydroxylation of coumarin to 7-hydroxycoumarin over WO_3 and
284 $\text{Pt-C}_3\text{N}_4$ under visible light is shown in Figure 4. As can be seen, minimal conversion of
285 coumarin was observed over both $\text{Pt-C}_3\text{N}_4$ and WO_3 , which was also supported by the
286 low formation of 7-hydroxycoumarin (Figure 5). $\text{Pt-C}_3\text{N}_4$ displayed a slow yet steady
287 conversion rate, reaching a 0.91 % drop in coumarin after 120 mins of irradiation
288 whereas, a varying coumarin concentration pattern was seen over time on WO_3 . It is
289 interesting to note that there was an initial decrease in coumarin concentration followed
290 by an increase which may be attributed to coumarin desorption from the surface of

291 WO₃. This desorption could be a result of the alteration in equilibrium in the closed
292 system due to the possible evolution of O₂ from water on WO₃ under visible light.

293

294 **Figure 4.**

295

296 While the decrease in coumarin concentration is low, production of OH radicals
297 over Pt-C₃N₄ and WO₃ was supported by the detection of 7-hydroxycoumarin upon
298 photocatalysis (Figure 5). When WO₃ was used as the photocatalyst, there was no 7-
299 hydroxycoumarin production until 30 minutes of irradiation which could be due to the
300 rapid recombination of the electrons and the photo generated holes. After 30 minutes,
301 OH radical production was steady with a gradual generation of 7-hydroxycoumarin
302 being observed. In the case of Pt-C₃N₄ however, 7-hydroxycoumarin production was
303 seen from 15 minutes. The initial increase in the 7-hydroxycoumarin concentration
304 correlates to a rapid degradation of coumarin during the first 60 mins of irradiation.

305

306 **Figure 5.**

307

308 In contrast to Pt-C₃N₄ and WO₃, the catalysts LaCr-SrTiO₃, Cr-SrTiO₃ and yellow
309 TiO₂ displayed no activity towards coumarin conversion to 7-hydroxycoumarin, which
310 indicates no OH radical formation. Furthermore, under prolonged visible light irradiation
311 no detectable 7-hydroxycoumarin was recorded.

312

313 **3.2.3 Influence of photocatalysts' electronic structure and particle size on OH** 314 **radical formation**

315 In order to evaluate and discuss the performance of the catalysts, it is essential to
316 consider the primary contributing factors; electronic structure and particle size. The
317 electronic structure of the catalysts dictates the initial photo-excitation of electrons to

318 higher energy levels, while the particle size dictates the concentration of photons
319 absorbed and surface reactions between coumarin and OH radicals. As shown in
320 reactions (2) – (6), OH radicals can occur via two routes in photocatalysis. The direct
321 formation at the valence band requires a redox potential of 2.8 V vs NHE, while the
322 indirect method occurs via the intermediate radical, $O_2^{\cdot-}$ and requires a redox potential
323 of -0.33 V vs NHE [53]. The electronic structure of the catalysts tested in this study, in
324 relation to the redox potentials required for radical formation, are shown in Figure 6.

325

326 **Figure 6**

327

328 As Figure 6 shows, catalysts TiO_2 P25, $Pt-C_3N_4$ and WO_3 possess an electronic
329 structure which corresponds to the redox potential of OH radical formation via either
330 direct or indirect mechanisms. The favourable electronic structure of TiO_2 for OH
331 radical formation has been well documented and is evident from the results highlighted
332 here. The performance of $Pt-C_3N_4$ and WO_3 for OH radical formation, however, has not
333 been as well reported. The structure of WO_3 with a more positive valence band
334 suggests it is capable of generating surface OH radicals, however, the results obtained
335 indicate minimal 7-hydroxycoumarin production within 2 hours. Based on the structure,
336 it was likely an increased rate of recombination preventing OH radical formation via the
337 valence band hole, due to insufficient energy to initiate a reduction reaction at the
338 conduction band [21]. To prevent recombination and to increase the OH radical
339 production, Kim *et al.* synthesised Pt-doped WO_3 and found that the OH radical
340 production from Pt- WO_3 was significantly higher than un-doped WO_3 [20]. Furthermore,
341 the large particle size of approximately 100 nm for WO_3 indicates a smaller surface
342 area, which leads to minimum absorption of light.

343

344 The electronic structure of Pt-C₃N₄ as seen from Figure 6 clearly indicates a
345 reducing catalyst, which is also supported by its application in water reduction
346 investigations [54]. Therefore, the hydroxylation of coumarin and subsequent formation
347 of 7-hydroxycoumarin, as indicated by the earlier results, is likely via the indirect O₂⁻
348 pathway. Based upon this observation, it is likely the low yield of OH radicals is a result
349 of competition for the conduction band electron between superoxide formation and H⁺
350 reduction to form H₂ (0 V vs NHE). In addition, since all these experiments were
351 performed in a closed system with limited O₂, a reducing catalyst such as Pt-C₃N₄ is
352 expected to produce less OH radicals than an open system. Furthermore, despite a
353 favourable particle size of 20-40 nm, Pt-C₃N₄ was observed to agglomerate to form
354 larger aggregates leading to a decrease in surface area and in turn light absorption.

355

356 In the case of LaCr-SrTiO₃, Cr-SrTiO₃ and yellow TiO₂, the electronic structures
357 showed both the valence band and conduction band of all these catalysts to be lower
358 than the redox potentials to facilitate radical formation as seen in Figure 6. These
359 catalysts were primarily used as a control parameter to ensure no 7-hydroxycoumarin
360 formation was observed.

361

362 The calculated OH radical concentrations and production rates produced over all
363 catalysts screened are summarised in Table 1. The results show that the activity of the
364 visible light activated photocatalysts studied were significantly lower than commercial
365 P25 under UV light. This further emphasises that although there are numerous visible
366 light absorbing photocatalysts, their ability to produce OH radicals is significantly lower
367 than P25. In future, if any visible light absorbing photocatalysts are to be fabricated for
368 the purpose of photocatalytic oxidation, their OH radical producing rates (and
369 quantities) should be determined and compared to P25 as demonstrated here.

370

371 **Table 1**

372

373 **4. CONCLUSION**

374 The aim of screening UV and visible light absorbing photocatalysts to assess their
375 oxidative strength was accomplished successfully by trapping OH radicals produced by
376 the photocatalysts in 7-hydroxycoumarin. The OH radical production capabilities of
377 various photocatalysts covering a range of band gaps and particle sizes were assessed
378 by comparing and discussing their differences with the commercial UV light activated
379 P25. To conclude, visible light activated photocatalysts such as LaCr-SrTiO₃, Cr-
380 SrTiO₃ and yellow TiO₂ did not produce any OH radicals and this could be attributed to
381 their electronic structure. Whereas, the (pseudo) maximum OH radical production rates
382 of other visible light activated photocatalysts namely, WO₃ (0.28 μM/hr) and Pt-C₃N₄
383 (0.886 μM/hr) were found to be significantly lower when compared to the commercial
384 UV light activated P25 photocatalyst (35.654 μM/hr). This method could be further
385 exploited as novel photocatalysts are developed and to compare a range of P25
386 concentrations for OH radical production. This study further emphasises the challenges
387 faced by the visible light photocatalysts for photocatalytic oxidation.

388

389 **5. ACKNOWLEDGEMENTS**

390 This work was supported by the Engineering and Physical Sciences Research
391 Council (Project number EP/K036769/1), Robert Gordon University's IDEAS PhD
392 studentship and Queen's University Belfast's PhD studentship. The author would also
393 like to thank Professor A Prasanna de Silva, School of Chemistry and Chemical
394 Engineering, Queen's University Belfast, for his valuable contribution during the
395 progress meetings. Supporting data are openly available on Queen's University,
396 Belfast Research Portal, [http:// pure.qub.ac.uk/portal/en/datasets/search.html](http://pure.qub.ac.uk/portal/en/datasets/search.html).

397

398 **REFERENCES**

- 399 [1] A. Fujishima, K. Honda, Electrochemical Photolysis of Water at a Semiconductor
400 Electrode, *Nature*. 238 (1972) 37-38.
- 401 [2] D.W. Bahnemann, L.A. Lawton, P.K.J. Robertson, The Application of
402 Semiconductor Photocatalysis for the Removal of Cyanotoxins from Water and Design
403 Concepts for Solar Photocatalytic Reactors for Large Scale Water Treatment, in: S.L.
404 Suib (Ed.), *New and Future Developments in Catalysis*, 1st ed., Elsevier, Amsterdam,
405 2013, pp. 395-415.
- 406 [3] M.R. Hoffmann, S.T. Martin, W. Choi, D.W. Bahnemann, *Environmental*
407 *Applications of Semiconductor Photocatalysis*, *Chem. Rev.* 95 (1995) 69-96.
- 408 [4] P.K.J. Robertson, J.M.C. Robertson, D.W. Bahnemann, Removal of
409 microorganisms and their chemical metabolites from water using semiconductor
410 photocatalysis, *J. Hazard. Mater.* 211–212 (2012) 161-171.
- 411 [5] H. Kominami, S. Murakami, M. Kohno, Y. Kera, K. Okada, B. Ohtani, Stoichiometric
412 decomposition of water by titanium(IV) oxide photocatalyst synthesized in organic
413 media: Effect of synthesis and irradiation conditions on photocatalytic activity, *Phys.*
414 *Chem. Chem. Phys.* 3 (2001) 4102-4106.
- 415 [6] C. McCullagh, P.K.J. Robertson, M. Adams, P.M. Pollard, A. Mohammed,
416 Development of a slurry continuous flow reactor for photocatalytic treatment of
417 industrial waste water, *J. Photochem. Photobiol. A*. 211 (2010) 42-46.
- 418 [7] P.K.J. Robertson, Semiconductor photocatalysis: an environmentally acceptable
419 alternative production technique and effluent treatment process, *J. Clean. Prod.* 4
420 (1996) 203-212.
- 421 [8] M. Adams, I. Campbell, C. McCullagh, D. Russell, D.W. Bahnemann, P.K.J.
422 Robertson, From Ideal Reactor Concepts to Reality: The Novel Drum Reactor for
423 Photocatalytic Wastewater Treatment, *Int. J. Chem. React. Eng.* 11 (2013) 621-632.
- 424 [9] O. Carp, C.L. Huisman, A. Reller, Photoinduced reactivity of titanium dioxide,
425 *Progress in Solid State Chemistry*. 32 (2004) 33-177.
- 426 [10] C. McCullagh, N. Skillen, M. Adams, P.K.J. Robertson, Photocatalytic reactors for
427 environmental remediation: a review, *J. Chem. Technol. Biotechnol.* 86 (2011) 1002-
428 1017.
- 429 [11] J. Jiang, Z. Zhou, V.K. Sharma, Occurrence, transportation, monitoring and
430 treatment of emerging micro-pollutants in waste water — A review from global views,
431 *Microchem. J.* 110 (2013) 292-300.
- 432 [12] A. Asghar, A.A. Abdul Raman, W.M.A. Wan Daud, Advanced oxidation processes
433 for in-situ production of hydrogen peroxide/hydroxyl radical for textile wastewater
434 treatment: a review, *J. Clean. Prod.* 87 (2015) 826-838.

- 435 [13] H. Fan, G. Li, F. Yang, L. Yang, S. Zhang, Photodegradation of cellulose under UV
436 light catalysed by TiO₂, *J. Chem. Technol. Biotechnol.* 86 (2011) 1107-1112.
- 437 [14] E. Szabó-Bárdos, K. Somogyi, N. Törő, G. Kiss, A. Horváth, Photocatalytic
438 decomposition of L-phenylalanine over TiO₂: Identification of intermediates and the
439 mechanism of photodegradation, *Appl. Catal. B: Environ.* 101 (2011) 471-478.
- 440 [15] T. Hirakawa, K. Yawata, Y. Nosaka, Photocatalytic reactivity for O₂⁻ and OH
441 radical formation in anatase and rutile TiO₂ suspension as the effect of H₂O₂ addition,
442 *Appl. Catal. A-Gen.* 325 (2007) 105-111.
- 443 [16] Y. Nosaka, T. Daimon, A.Y. Nosaka, Y. Murakami, Singlet oxygen formation in
444 photocatalytic TiO₂ aqueous suspension, *Phys. Chem. Chem. Phys.* 6 (2004) 2917-
445 2918.
- 446 [17] X. Yan, T. Ohno, K. Nishijima, R. Abe, B. Ohtani, Is methylene blue an appropriate
447 substrate for a photocatalytic activity test? A study with visible-light responsive titania,
448 *Chemical Physics Letters.* 429 (2006) 606-610.
- 449 [18] B. Ohtani, Preparing Articles on Photocatalysis—Beyond the Illusions,
450 Misconceptions, and Speculation, *Chem. Lett.* 37 (2008) 216-229.
- 451 [19] A. Mills, An overview of the methylene blue ISO test for assessing the activities of
452 photocatalytic films, *Applied Catalysis B: Environmental.* 128 (2012) 144-149.
- 453 [20] J. Kim, C.W. Lee, W. Choi, Platinized WO₃ as an Environmental Photocatalyst that
454 Generates OH Radicals under Visible Light, *Environ. Sci. Technol.* 44 (2010) 6849-
455 6854.
- 456 [21] Q. Xiang, J. Yu, P.K. Wong, Quantitative characterization of hydroxyl radicals
457 produced by various photocatalysts, *J. Colloid Interface Sci.* 357 (2011) 163-167.
- 458 [22] M. Sato, T. Ohgiyama, J.S. Clements, Formation of chemical species and their
459 effects on microorganisms using a pulsed high voltage discharge in water, *Industry*
460 *Applications Society Annual Meeting.* 2 (1994) 1455-1461.
- 461 [23] H. Czili, A. Horváth, Applicability of coumarin for detecting and measuring hydroxyl
462 radicals generated by photoexcitation of TiO₂ nanoparticles, *Appl. Catal. B: Environ.* 81
463 (2008) 295-302.
- 464 [24] R. Ono, T. Oda, Measurement of hydroxyl radicals in pulsed corona discharge, *J.*
465 *Electrostatics.* 55 (2002) 333-342.
- 466 [25] W. Hoeben, E. van Veldhuizen, W. Rutgers, G. Kroesen, Gas phase corona
467 discharges for oxidation of phenol in an aqueous solution, *J. Phys. D: Appl. Phys.* 32
468 (1999) 133-137.
- 469 [26] P. Sunka, V. Babický, M. Clupek, P. Lukes, M. Simek, J. Schmidt, M. Cern,
470 Generation of chemically active species by electrical discharges in water, *Plasma*
471 *Sources Sci. Technol.* 8 (1999) 258-265.

- 472 [27] B. Sun, M. Sato, J. Sid Clements, Optical study of active species produced by a
473 pulsed streamer corona discharge in water, *J. Electrostatics*. 39 (1997) 189-202.
- 474 [28] M.G. Steiner, C.F. Babbs, Quantitation of the hydroxyl radical by reaction with
475 dimethyl sulfoxide, *Arch. Biochem. Biophys.* 278 (1990) 478-481.
- 476 [29] M. Sahni, B.R. Locke, Quantification of Hydroxyl Radicals Produced in Aqueous
477 Phase Pulsed Electrical Discharge Reactors, *Ind. Eng. Chem. Res.* 45 (2006) 5819-
478 5825.
- 479 [30] J. Ku, E. Zimowski, United States Department of Labor, Occupational Safety and
480 Health Administration. 3M Formaldehyde Monitor (Model 3721), Product evaluation
481 (PE-10). 205 (1989).
- 482 [31] S.A.V. Eremia, D. Chevalier-Lucia, G. Radu, J. Marty, Optimization of hydroxyl
483 radical formation using TiO₂ as photocatalyst by response surface methodology,
484 *Talanta*. 77 (2008) 858-862.
- 485 [32] T. Maezono, M. Tokumura, M. Sekine, Y. Kawase, Hydroxyl radical concentration
486 profile in photo-Fenton oxidation process: Generation and consumption of hydroxyl
487 radicals during the discoloration of azo-dye Orange II, *Chemosphere*. 82 (2011) 1422-
488 1430.
- 489 [33] M. Tokumura, R. Morito, R. Hatayama, Y. Kawase, Iron redox cycling in hydroxyl
490 radical generation during the photo-Fenton oxidative degradation: Dynamic change of
491 hydroxyl radical concentration, *Appl. Catal. B: Environ.* 106 (2011) 565-576.
- 492 [34] S. Kanazawa, T. Furuki, T. Nakaji, S. Akamine, R. Ichiki, Measurement of OH
493 Radicals in Aqueous Solution Produced by Atmospheric-pressure LF Plasma Jet, *I. J.*
494 *PEST*. 6 (2012) 166-171.
- 495 [35] K. Ishibashi, A. Fujishima, T. Watanabe, K. Hashimoto, Quantum yields of active
496 oxidative species formed on TiO₂ photocatalyst, *J. Photochem. Photobiol. A*. 134
497 (2000) 139-142.
- 498 [36] T. Hirakawa, Y. Nosaka, Properties of O₂⁻ and OH[•] Formed in TiO₂ Aqueous
499 Suspensions by Photocatalytic Reaction and the Influence of H₂O₂ and Some Ions,
500 *Langmuir*. 18 (2002) 3247-3254.
- 501 [37] Z. Li, T. Liang, S. Lv, Q. Zhuang, Z. Liu, A Rationally Designed Upconversion
502 Nanoprobe for in Vivo Detection of Hydroxyl Radical, *J. Am. Chem. Soc.* 137 (2015)
503 11179-11185.
- 504 [38] J. Zhang, Y. Nosaka, Quantitative Detection of OH Radicals for Investigating the
505 Reaction Mechanism of Various Visible-Light TiO₂ Photocatalysts in Aqueous
506 Suspension, *J. Phys. Chem. C*. 117 (2013) 1383-1391.
- 507 [39] M.E. Lindsey, M.A. Tarr, Quantitation of hydroxyl radical during Fenton oxidation
508 following a single addition of iron and peroxide, *Chemosphere*. 41 (2000) 409-417.

- 509 [40] J. Zhang, Y. Nosaka, Generation of OH radicals and oxidation mechanism in
510 photocatalysis of WO₃ and BiVO₄ powders, *J. Photochem. Photobiol. A.* 303–304
511 (2015) 53-58.
- 512 [41] F. Fina, H. Menard, J.T.S. Irvine, The effect of Pt NPs crystallinity and distribution
513 on the photocatalytic activity of Pt-g-C₃N₄, *Phys. Chem. Chem. Phys.* 17 (2015)
514 13929-13936.
- 515 [42] C. Randorn, J.T.S. Irvine, P. Robertson, Synthesis of Visible-Light-Activated
516 Yellow Amorphous Photocatalyst, *Int. J. Photoenergy.* 2008 (2008) 1-6.
- 517 [43] S. Ouyang, H. Tong, N. Umezawa, J. Cao, P. Li, Y. Bi, Y. Zhang, J. Ye, Surface-
518 Alkalinization-Induced Enhancement of Photocatalytic H₂ Evolution over SrTiO₃-Based
519 Photocatalysts, *J. Am. Chem. Soc.* 134 (2012) 1974-1977.
- 520 [44] M. Muralidharan, V. Anbarasu, A. Elaya Perumal, K. Sivakumar, Carrier mediated
521 ferromagnetism in Cr doped SrTiO₃ compounds, *J. Mater. Sci. : Mater. Electron.* 26
522 (2015) 6352-6365.
- 523 [45] J. Guo, Y. Li, S. Zhu, Z. Chen, Q. Liu, D. Zhang, W. Moon, D. Song, Synthesis of
524 WO₃@Graphene composite for enhanced photocatalytic oxygen evolution from water,
525 *RSC Adv.* 2 (2012) 1356-1363.
- 526 [46] K. van Benthem, C. Elsässer, R.H. French, Bulk electronic structure of SrTiO₃:
527 Experiment and theory, *J. Appl. Phys.* 90 (2001) 6156-6164.
- 528 [47] J. Kamalakkannan, V.L. Chandraboss, S. Prabha, S. Senthilvelan, Advanced
529 construction of heterostructured InCrO₄-TiO₂ and its dual properties of greater UV-
530 photocatalytic and antibacterial activity, *RSC Adv.* 5 (2015) 77000-77013.
- 531 [48] M. Wojtoniszak, B. Zielinska, R.J. Kalenczuk, E. Mijowska, Photocatalytic
532 performance of titania nanospheres deposited on graphene in coumarin oxidation
533 reaction, *Materials Science-Poland.* 30 (2012) 32-38.
- 534 [49] G. Li, K.H. Wong, X. Zhang, C. Hu, J.C. Yu, R.C.Y. Chan, P.K. Wong, Degradation
535 of Acid Orange 7 using magnetic AgBr under visible light: The roles of oxidizing
536 species, *Chemosphere.* 76 (2009) 1185-1191.
- 537 [50] J. Zhang, Y. Nosaka, Mechanism of the OH Radical Generation in Photocatalysis
538 with TiO₂ of Different Crystalline Types, *J. Phys. Chem. C.* 118 (2014) 10824-10832.
- 539 [51] H. Guan, L. Zhu, H. Zhou, H. Tang, Rapid probing of photocatalytic activity on
540 titania-based self-cleaning materials using 7-hydroxycoumarin fluorescent probe, *Anal.*
541 *Chim. Acta.* 608 (2008) 73-78.
- 542 [52] Z. Huang, Q. Sun, K. Lv, Z. Zhang, M. Li, B. Li, Effect of contact interface between
543 TiO₂ and g-C₃N₄ on the photoreactivity of g-C₃N₄/TiO₂ photocatalyst: (0 0 1) vs (1 0
544 1) facets of TiO₂, *Applied Catalysis B: Environmental.* 164 (2015) 420-427.
- 545 [53] P.M. Wood, The potential diagram for oxygen at pH 7, *Biochem. J.* 253 (1988)
546 287-289.

547 [54] G. Zhang, Z. Lan, L. Lin, S. Lin, X. Wang, Overall water splitting by Pt/g-C₃N₄
548 photocatalysts without using sacrificial agents, Chem. Sci. 7 (2016) 3062-3066.

549

550 **List of Captions for figures and tables.**

551 Figure 1: XRD profiles of photocatalysts representing the plane indices [44,45].

552 Figure 2: UV-Visible absorption spectra of photocatalysts

553 Figure 3: Coumarin and 7-hydroxycoumarin profiles of 100 ml of 100 μ M coumarin with
554 0.1 g/L P25 under 36 W UV light

555 Figure 4: Coumarin profiles of 100 ml of 100 μ M coumarin with 0.1 g/L visible light
556 photocatalysts; Inset: coumarin profiles of WO_3 and Pt- C_3N_4

557 Figure 5: 7-hydroxycoumarin production profiles of 100 ml of 100 μ M coumarin with 0.1
558 g/L visible light photocatalysts

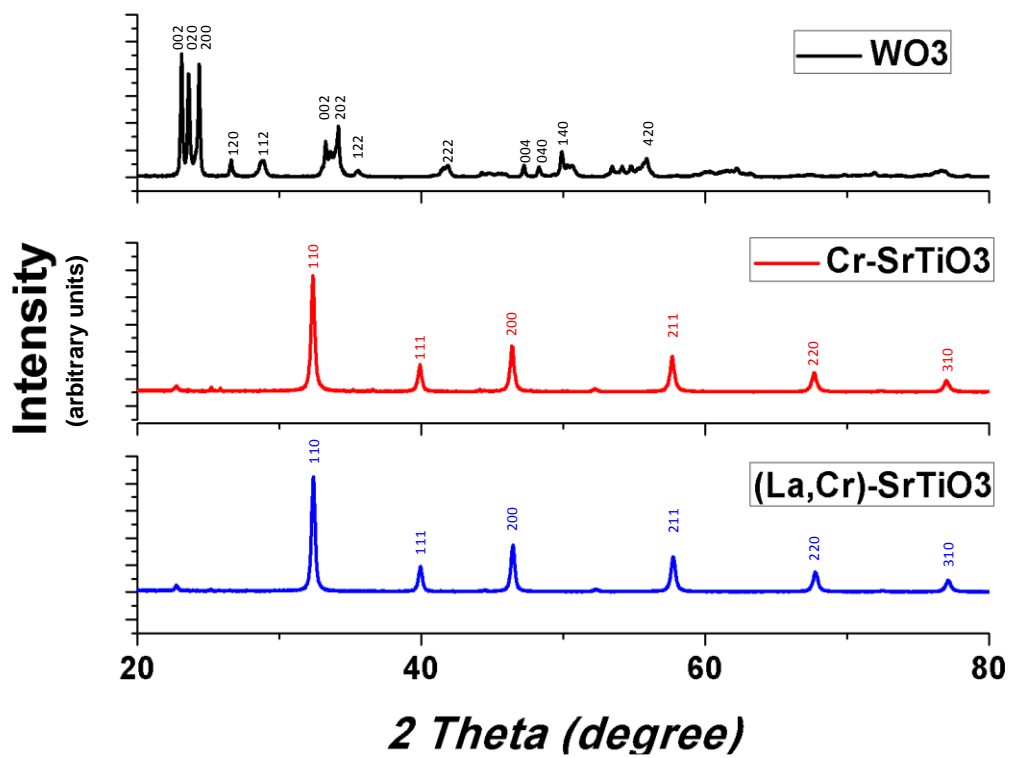
559 Figure 6: Electronic structure of the photocatalysts used

560

561 Table 1: Pseudo maximum OH radical production rates and quantities.

562

563



564

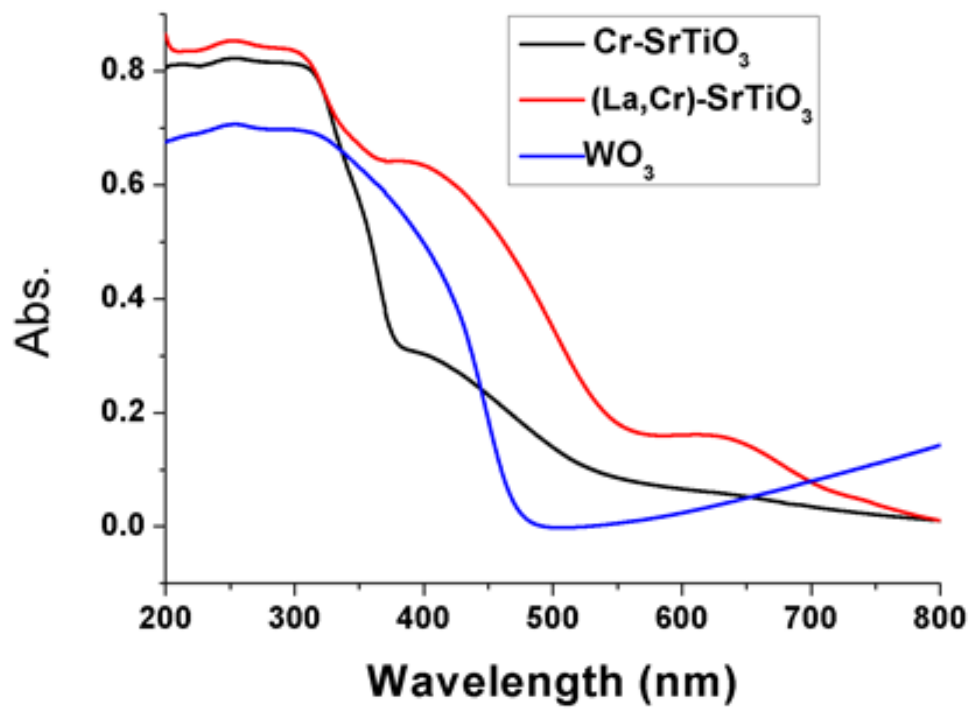
565 **Figure 1**

566

567

568

569



570

571 **Figure 2**

572

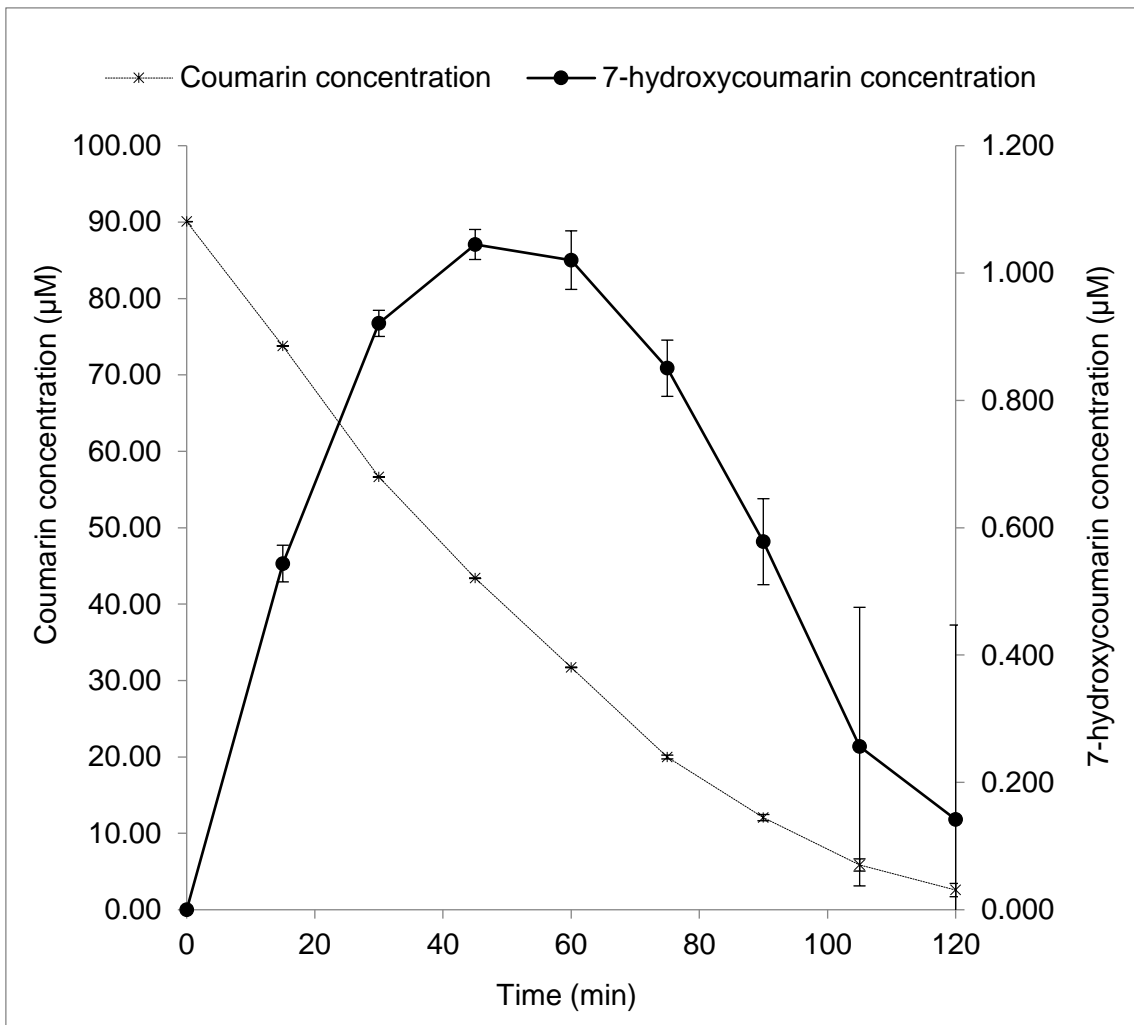
573

574

575

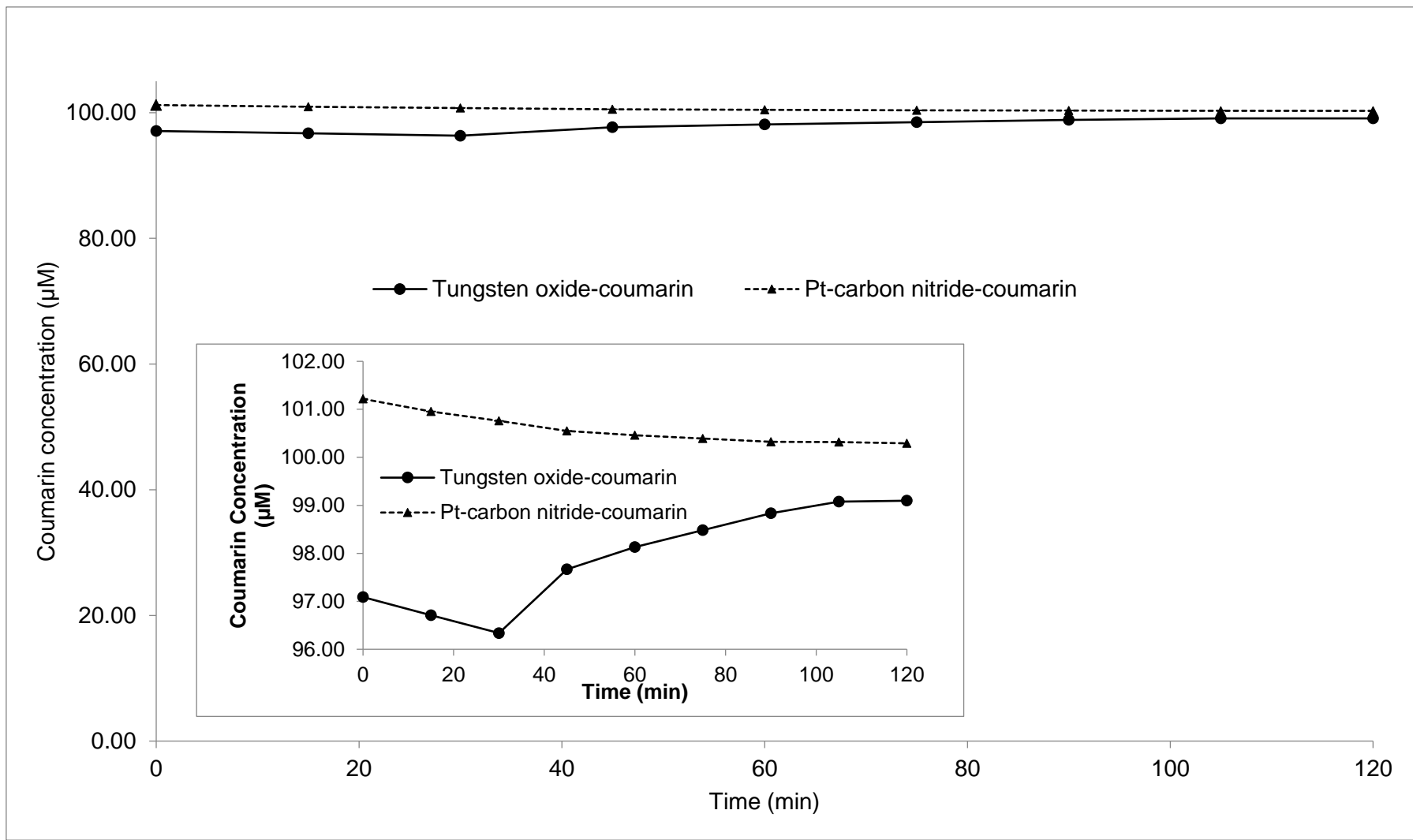
576

577



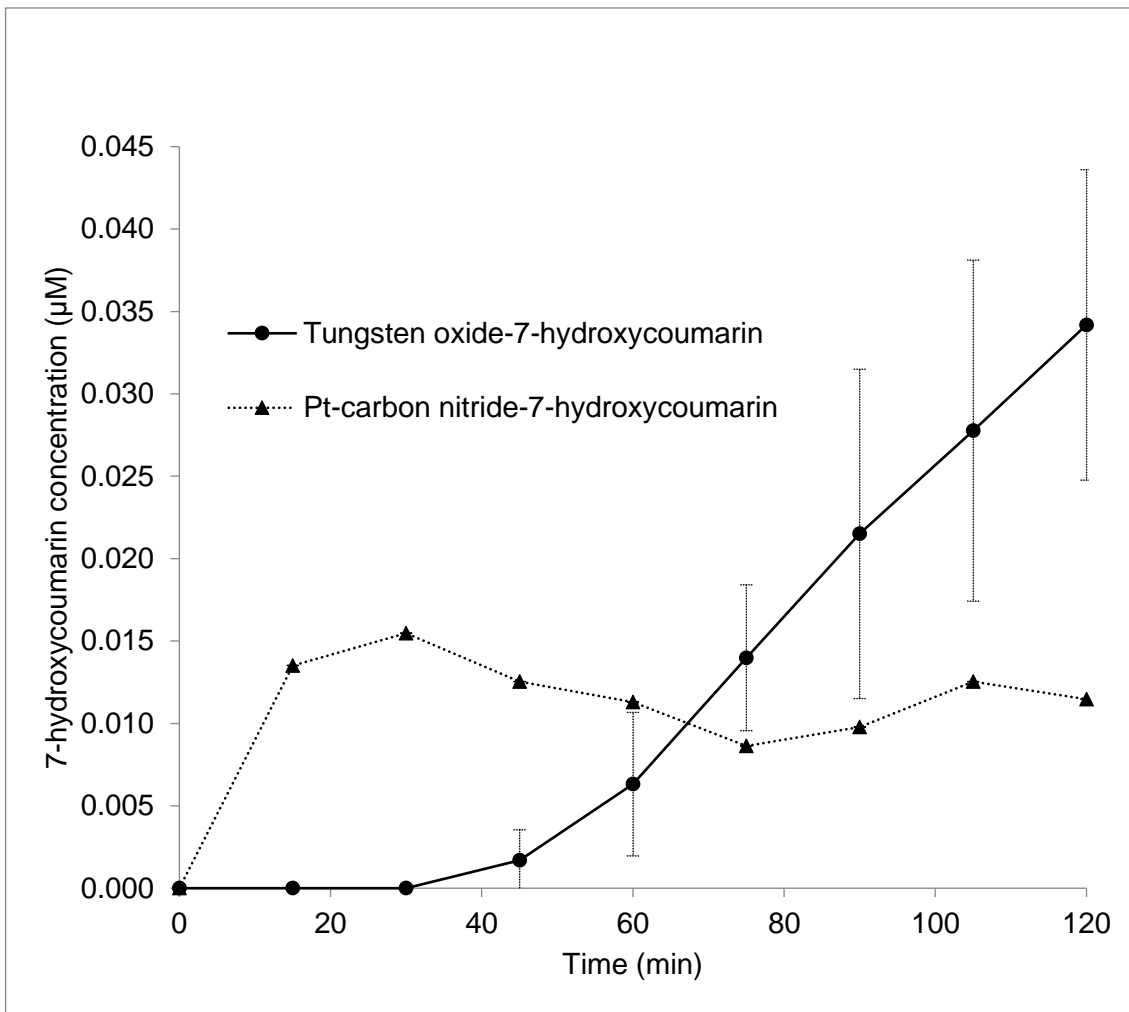
578

579 **Figure 3**



580

581 **Figure 4**



582

583 **Figure 5**

584

585

586

587

588

589

590

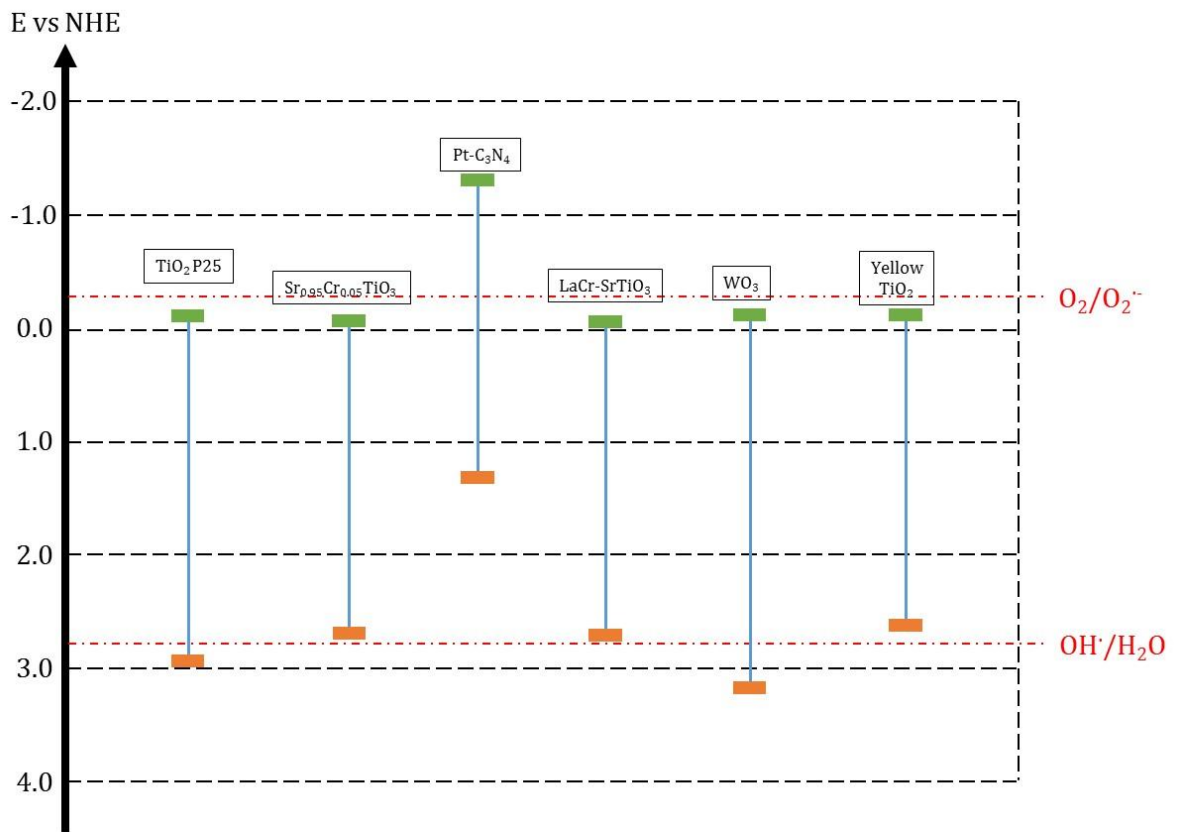
591

592

593

594

595



596

597

598 **Figure 6**

599

600

601

602

603

604

605

606

607

608

Photocatalyst	Light Source	Maximum OH radical concentration (μM)	Time at which maximum concentration of OH radical was produced (min)	Maximum OH radical production rate ($\mu\text{M/hr}$)
P25	UV	16.9	45	35.654
WO ₃	visible	0.560	120	0.280
Pt-C ₃ N ₄	visible	0.254	30	0.886

609

610 **Table 1**